The Prostate

WILEY

The Prostate

ORIGINAL ARTICLE

Automatic MRI-TRUS Fusion Technique for Transperineal Biopsy Guidance: From Preoperative Planning to Intraoperative Navigation

Lu Tang[1] | Menglin Wu[2,3] | Ke Chen[1,4] | Fan Gao[1,5] | Baohui Zheng[1] | Shu Zhao[3,6] | Pablo D. Burstein[3] | Sikai Ge[7] | Xu Zhang[1] | Jie Zhu[1]

[1]Senior Department of Urology, The Third Medical Center of Chinese PLA General Hospital, Beijing, China | [2]School of Computer Science and Technology, Nanjing Tech University, Nanjing, China | [3]Carbon Medical Device Ltd, Shenzhen, China | [4]Department of Urology, Chinese PLA The 96601 Military Hospital, Huangshan, China | [5]School of Medicine, Nankai University, Tianjin, China | [6]School of Medicine, Zhejiang University, Hangzhou, China | [7]School of Mathematics and Physics, Xi'an Jiaotong-Liverpool University, Suzhou, China

Correspondence: Sikai Ge (sikai.ge21@student.xjtlu.edu.cn) | Xu Zhang (xzhang301@163.com) | Jie Zhu (zhu_xiaocen@163.com)

Received: 4 July 2024 | **Revised:** 22 November 2024 | **Accepted:** 10 December 2024

Funding: The authors received no specific funding for this work.

Keywords: biopsy procedures | image-guided | prostate cancer

ABSTRACT

Background: Targeted and systematic transperineal biopsy of lesions guided by magnetic resonance imaging (MRI) and transrectal ultrasonography (TRUS) fusion technique may optimize the biopsy procedure and enhance the detection of prostate cancer. We described the transperineal biopsy guided by an automatic MRI-TRUS fusion technique, and evaluated the accuracy and feasibility of this method in a prospective single-center study.

Methods: The proposed method focuses on automating the delineation of prostate contours in both the MRI and TRUS images, the registration and fusion of MRI and TRUS images, the generation and visualiztion of the systematic biopsy cores in their corresponding locations within the 2D and the 3D views, as well as the computation and visualiztion of needle trajectories from preoperative planning to intraoperative navigation. A total of 76 patients with clinically suspected prostate cancer underwent systematic (SBx) and targeted (TBx) biopsies, all performed by a single urologist with more than 10 years of experience. The detection rates of prostate cancer (PCa) and clinically significant prostate cancer (csPCa) were recorded. We also measured preoperative registration time, duration of the overall surgical procedure, and postoperative complication rates within the first week following the surgery. Descriptive analyses were presented in this study.

Results: PCa was identified in 73.7% (56/76) of the subjects, while csPCa was identified in 61.8% (47/76). The preoperative registration time was 5.0 min (IQR: 4.4–6.0), while the overall surgery duration was 24.8 min (IQR: 23.2–27.2). Postoperatively, 12 patients experienced immediate hematuria, and one patient reported dysuria 1 day following surgery.

Conclusions: The automatic MRI-TRUS fusion technique for transperineal biopsy is feasible and safe, with preoperative planning to intraoperative navigation it offering convenient and efficient preoperative preparation and surgical procedure.

In this study, we developed an innovative automatic MRI-TRUS fusion and navigation biopsy technique, and evaluated its effectiveness and safety in a clinical trial using transperineal prostate biopsy. Ths novel guided biopsy system significantly reduces procedure time, decreases user variability, and potentially enhances fusion accuracy.

1 | Introduction

Prostate cancer (PCa) is the most common malignant tumor in the male genitourinary system [1]. According to the 2022 global cancer statistics from the World Health Organization, there are approximately 1.4 million new cases and 396,792 deaths of PCa worldwide [2]. In the past decades, approaches and technologies such as prostate-specific antigen (PSA), digital rectal examination (DRE), and multi-parametric magnetic resonance imaging (mpMRI) have played important roles in PCa diagnosis [3], while the gold standard for diagnosing PCa remains prostate biopsy histopathological examination.

Nowadays, prostate biopsy can be conducted using either the transperineal (TP) or transrectal (TR) approaches, with the prostate and biopsy procedure being monitored by transrectal ultrasonography (TRUS). For the TR approach, biopsy needles are inserted through the rectal wall into the prostate parenchyma under the guidance of a TRUS probe. During TP process, the direction of the biopsy needle remains parallel to the TRUS probe and the needle enters through the perineum, while the probe's longitudinal (sagittal) plane is oriented to scan the target biopsy area [3]. Compared to transrectal biopsy (TRB), transperineal biopsy (TPB) has fewer perioperative complications, as well as higher cancer detection rate both in the apex and transitional zone of the prostate [4–6].

Due to the inherent limitations of US imaging, patients undergoing TRUS (only)-guided biopsy are often at the risk of either underdiagnosis of clinically significant prostate cancer (csPCa), or overdiagnosis of clinically insignificant PCa [3]. The introduction of mpMRI-TRUS fusion before or during biopsy procedure helps reducing such risks due to the MRI scan's higher detail. Current technologies approach mpMRI-TRUS fusion either by cognitive fusion, where clinicians memorize lesions identified on mpMRI and mentally overlay them onto the corresponding ultrasound images, or software based fusion, where a dedicated software automatically overlays such lesions. The cognitive fusion approach is highly operator dependent, often leading to overlooking small lesions, and, as a consequence to a decrease in detection rates of csPCa [7].

With the development of artificial intelligence (AI) image processing technology, software based mpMRI-TRUS fusion enables the precise localization of mpMRI combined with the real-time imaging capabilities of ultrasound. This technique involves acquiring TRUS images of the prostate, which are subsequently fused with previously obtained MRI images to create a 3D prostate model [3]. Rigid and/or elastic registration techniques are implemented to ensure alignment of the mpMRI prostate volume with the TRUS volume. In addition, electromechanical or electromagnetic (EM) probe tracking is employed in the biopsy procedure. Generally, differences between present fusion platforms mainly concern the registration algorithm (rigid vs. elastic), the navigation strategy (organ-based vs. tracking), post-biopsy needle position recording, and the use of robotic arms [8].

Segmentation and registration methods commonly employed by most platforms are semi-automatic and/or require manual adjustment. For instance, when using Artemis (Eigen, Grass Valley, CA) for biopsy guiding, the first step consists in manually delineating the region of interest (ROI) on the (preop/offline) workstation. Subsequently, the MRI data, loaded into the Artemis device during the intervention, is manually aligned with the real-time US, generating a virtual 3D prostate model with ROIs overlaid on-the-fly [9]. Average time for registration/fusion was estimated to be less than 5 min [10]. Guided by the 3D model, TRB of target lesions and systematic biopsies are performed under local anesthesia [9]. Immerzeel et al. [11] also reported a TP MRI–TRUS fusion guided biopsy procedure under local anesthesia. Same as in Artemis, clinicians first manually delineate the prostate and suspected lesions on MRI using a contour software (MIM Symphony Dx; MIM, Cleveland, OH, USA), taking approximately 10–15 min per patient.

In terms of ultrasound tracking mechanism, numerous platforms use mechanical encoders, e.g. Artemis attaches the ultrasound probe to a tracking arm, while relatively few using EM or optical navigation [8]. While mechanical localizers are highly accurate, they are inherently limited to tracking a single object [12]. Also, they are, in general, relatively large and cumbersome for use in a small operating field [13]. In 2023, Fletcher et al. [14] reported a vector prostate biopsy system that comprises BiopSee fusion workstation (MedCom, Darmstadt, Germany), EM tracking technology, and TR ultrasound. In this procedure, stepper-mounted TRUS images were fused with MRI scans, and the biopsy needle was directed through the sheath to MRI targets under EM tracking. The procedure was validated in 69 patients, yielding a cancer detection in patients with Likert 4–5 lesions at 98% for anyPCa, and 83% for grade group (GG) ≥ 2.

The main drawbacks of manual or semi-automatic segmentation and registration are (1) the time it takes to label and align, and (2) the operator dependency when reading the scans. Some mechanical navigation systems offer a limited number of tracking targets, as well as a reduced number of degrees of freedom (DoF). Modern EM tracking system, on the other hand, do not suffer from these limitations.

In this study, we developed a novel MRI-TRUS fusion biopsy technique, which automatically delineates the prostate contour, registers and fuses MRI and TRUS images, creates systematic biopsy cores, computes needle trajectories, and integrates EM tracking to achieve precise intraoperative navigation. Lesion delineation remains flexible, allowing for clinician discretion.

To verify its effectiveness and safety, biopsies were performed on suspected PCa patients using our system.

2 | Materials and Methods

2.1 | Study Population

This study was approved by Chinese PLA General Hospital Institutional Ethics Committee (IEC No: S2023-135-02) and registered at the Chinese Clinical Trial Registry (ChiCTR2300072960). Detailed explanations of the informed consent and patient information sheet were provided to the study participants before their enrollment.

Patients with clinically suspected PCa were recruited and underwent systematic biopsies (SBx) with 12 cores, as well as targeted biopsies (TBx) with 1–3 cores using our system. Details on the inclusion and exclusion are provided in the Supporting Information material (Supporting Information S1: Table S1).

2.2 | Imaging

Patients enrolled underwent prebiopsy mpMRI using a 3.0 T system equipped with an 8-channel phased-array coil and without endorectal coil (Supporting Information S1: Table S2). The MRI sequences were assessed based on the Prostate Imaging-Reporting and Data System (PI-RADS) v2.1 criteria. In patients with PI-RADS scores of 3 lesions, the decision to perform a biopsy was augmented by additional factors including PSA velocity (doubling within 3 months) and PSA density (> 0.15 ng/mL/cm^3).

2.3 | System Design

The MRI-TRUS fusion biopsy system consists of a 3D reconstruction and planning software (Carbon Med, Shenzhen, CN) and the Venus PRO Diagnostic Ultrasound (Carbon Med, Shenzhen, CN) equipped with an image fusion surgical system (IFUSS). This system is integrated with a 3D guidance EM tracking module (Northern Digital Inc., Waterloo, CAN), tracking two sensors—one attached to the needle grip while the other to the bi-plane probe. The EM transmitter is positioned adjacent to the patient, within a range ensuring precise tracking of both the needle and probe. Bi-plane fused MRI-TRUS images, depicting the needle trajectory and biopsy cores in the sagittal plane, along with a 3D visualization, displaying needle grip, probe, prostate gland, pubic bone, lesions, and targets, facilitate real-time monitoring.

2.4 | Preoperative Planning

2.4.1 | Preoperative Preparation

The TPB was performed as an outpatient procedure with local anesthesia (1% lignocaine solution, Figure 4a, Supporting Information S1: Table S3) in the operating room. A single dose of antibiotic was administered as preoperative prophylaxis following a test dose 30 min before the procedure.

2.4.2 | Image Segmentation and Lesion Delineation

The mpMRI's corresponding scans, comprising T2-weighted, high b-value diffusion-weighted (DWI), and apparent diffusion coefficient (ADC), are loaded and overlaid to facilitate manual lesion delineation using our system's tools. Automatic prostate contour and pubic bone segmentations are obtained using a pretrained deep neural network (U-Net) [15] fed with T2-weighted sequences. The U-Net is a U-shaped encoder-decoder network with skip connections between mirrored layers in the encoder and decoder stacks, enabling alignment of the underlying structures in the input and output layers. Subsequently, the Marching Cubes algorithm generates a 3D surface mesh by extracting isosurfaces from the segmentations through a grid-based triangulation process [16]. Mesh filtering is then applied to refine the mesh, enhancing its smoothness and accuracy (Figure 1).

To conduct the endorectal ultrasonography, the patient was positioned in the lithotomy position, and the perineal skin was disinfected with iodophor. The probe is slowly inserted into the rectum to acquire axial prostate images, from base to apex, where the prostate contour is automatically segmented from.

2.4.3 | Image Registration and Fusion

Based on the prostate contours obtained in 2.4.2, and using the Iterative Closest Points (ICP) algorithm [17], the MRI is registered to the US (Figure 2), effectively aligning the MRI coordinate system to the EM tracking coordinate system. Guided by the probe's tracked position and orientation, transparency controlled fused sagittal and transverse images, overlapping US and MRI, are generated in real-time.

2.4.4 | Biopsy Protocol

Using mpMRI, including T2-weighted, DWI, and ADC sequences, identify suspicious PCa nodules, and label them as biopsy targets. Up to three nodules may be chosen as targets.

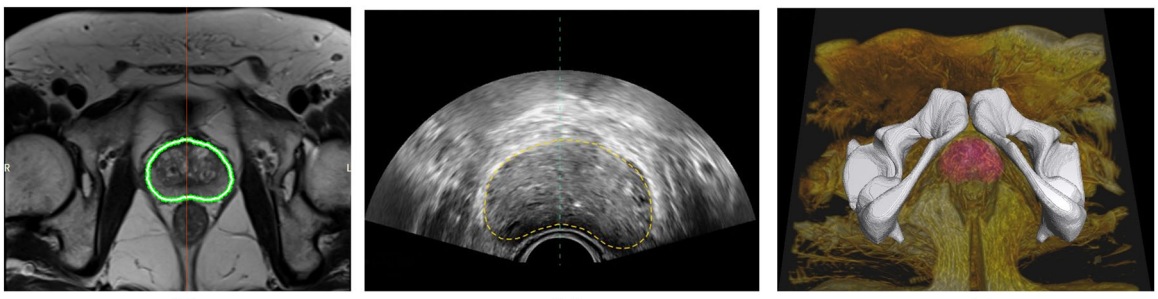

(a) (b) (c)

FIGURE 1 | Image segmentation and 3D reconstruction. (a) Prostate segmentation in MRI. (b) Prostate segmentation in ultrasound image. (c) 3D reconstruction of the prostate and pubic bone. [Color figure can be viewed at wileyonlinelibrary.com]

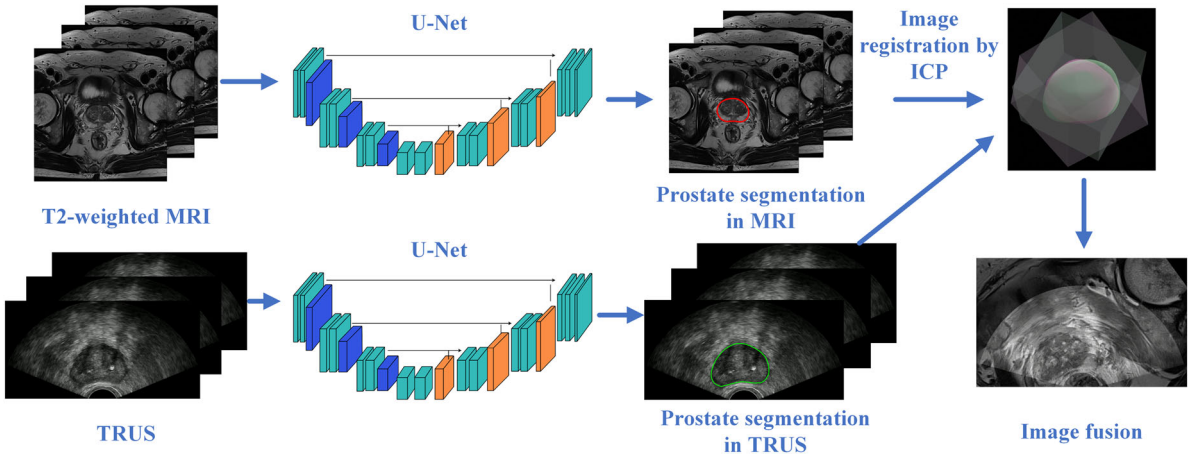

FIGURE 2 | The flowchart of the MRI-TRUS fusion technology. [Color figure can be viewed at wileyonlinelibrary.com]

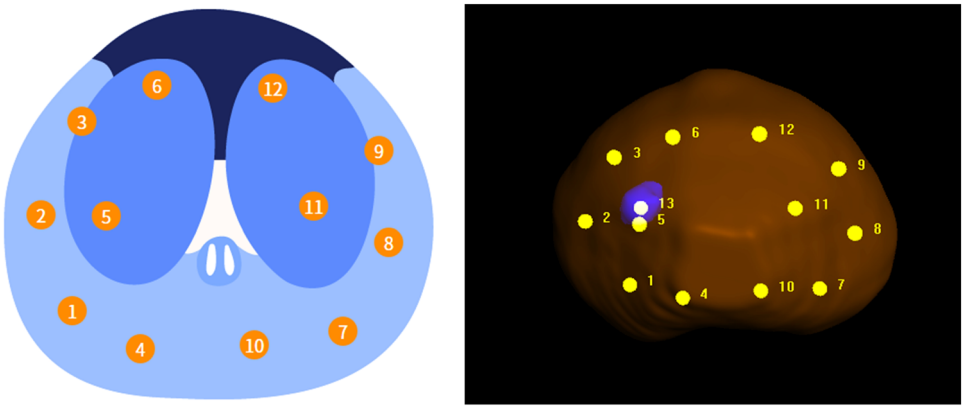

FIGURE 3 | Biopsy core planning. (a) A biopsy core distribution diagram based on Ginsburg protocol. (b) A 3D visualization of the biopsy cores for the real patient. The yellow points indicate the systematic cores, and the purple region denotes the suspicious area for targeted biopsy. [Color figure can be viewed at wileyonlinelibrary.com]

Patient specific SBx samples are automatically generated by mapping a standard biopsy core distribution diagram to the EM tracking coordinate system, its shaped deformed according to the patient specific prostate shape via the deformable registration method (Figure 3) [18].

2.5 | Intraoperative Navigation

2.5.1 | Navigation During Surgery

A color-coded, disposable needle-guide is attached to the TRUS probe for faster aim and physiscal support of the needle (Figure 4b, instert in Figure 4d). The projected needle-path is dynamically computed based on the relative spatial position of the probe (obtained from EM tracking) and the biopsy cores, and is shown on the sagittal TRUS image in real-time. To speed up needle-insertion, the numbered cores (targeted and systematic), and the corresponding needle-guide-matching, numbered and color-coded channels are also added to the sagittal TRUS image (Figure 4d). Needle-target alignment (computed from EM tracking) is highlighted in green both in the sagittal TRUS image and the 3D navigation panel, adding yet an extra layer of assistance (Figure 4c,d). Finally, to ensure prostatic tissue sample collection, and to avoid injuring unintended structures/organs, a *safety-zone*, in the form of a yellow dashed rectangle showing an estimate of the range of needle insertion, is displayed (Figure 4d).

2.5.2 | Target and Systematic Biopsy

TBx samples were taken first, with 1 needle for each PI-RADS score ≥ 3 lesions, followed by 12-needle SBx samples according to the Ginsburg protocol [19]. In cases where no target was identified on the MRI, but biopsy criteria were met, only SBx samples were taken. Biopsies were performed by one urologist with more than 10 years of experience performing prostate biopsies.

2.6 | Pathological Analysis

Biopsy cores were reported as the Gleason score and GG according to International Society of Urological Pathology (ISUP) standards [20], with csPCa defined as GG ≥ 2.

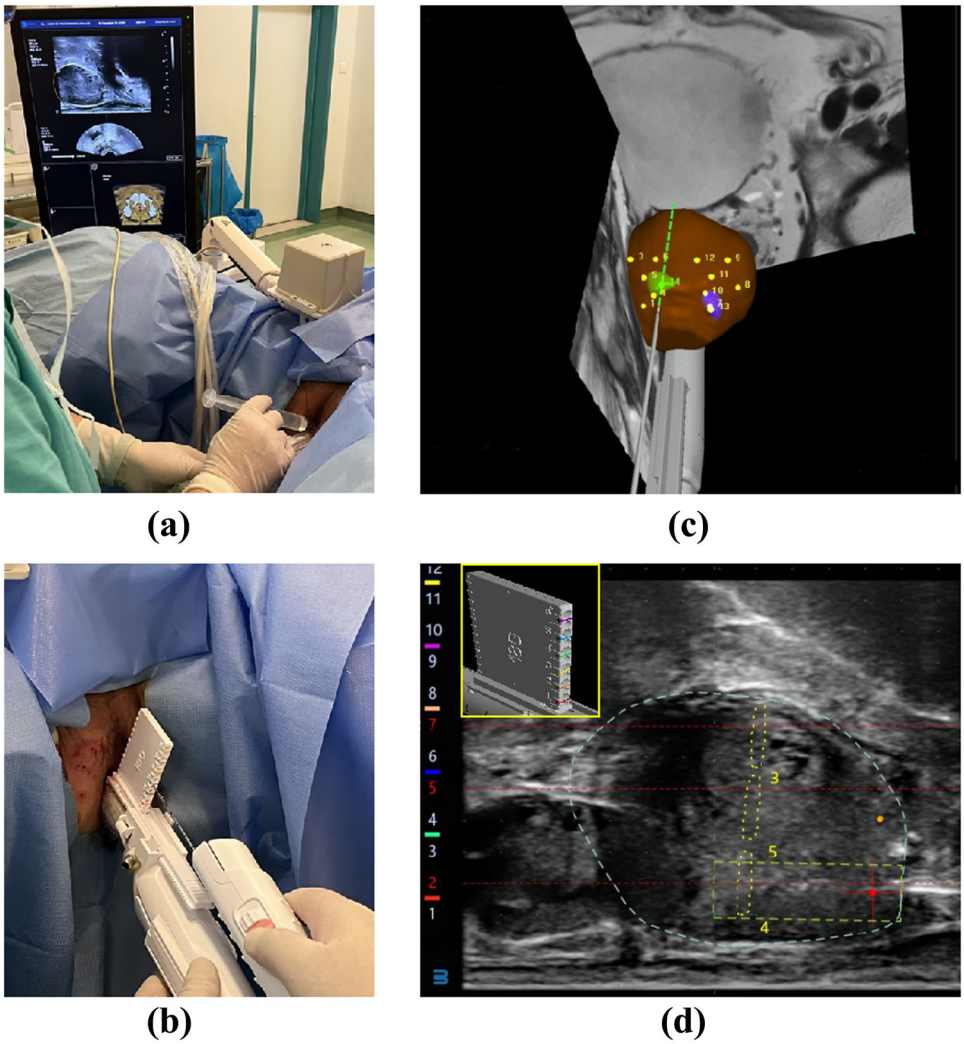

FIGURE 4 | Transperineal MRI-TRUS fusion-guided biopsy under electromagnetic navigation. (a) Perineal regional local anesthesia under transrectal ultrasound guidance. (b) Transperineal biopsy under electromagnetic navigation. (c) 3D visualization for surgical navigation. (d) The sagittal plane of the fused ultrasound image, displaying the prostate contour, suggested needle paths (red dashed line), numbered biopsy cores (yellow dashed oval), and safety zone. The disposable needle-guide is shown in the upper left corner. [Color figure can be viewed at wileyonlinelibrary.com]

2.7 | Post-Biopsy Evaluation

We monitored the patients for symptoms such as vomiting, pain, hematuria, urinary retention, infections, fever, hematochezia, hematospermia, and pain. All patients were assessed pain sense with the Visual Analogue Scale (VAS). The scoring criteria were as follows: 0 points for no pain; 1–3 points for mild but tolerable pain; 4–6 points for pain that is still bearable; 7–10 points for progressively intense pain that is hard to endure.

2.8 | Statistical Analysis

Statistical analysis was conducted utilizing SPSS software version 27.0.1.0 (IBM SPSS Statistics for Windows, Version 27.0.1.0. Armonk, NY: IBM Corp.). Descriptive analysis findings were presented in this study. Mean and standard deviation (SD) were used for normal distributed continuous variables, while medians and interquartile ranges (IQRs) were used for non-normal distribution. Numbers with percentages were used for categorical variables.

3 | Results

3.1 | Demographic Data

Table 1 presents the demographic and perioperative information of the cohort. Out of the initial 83 patients, one was excluded due to bilateral femoral head necrosis preventing lithotomy position procedure, six were unable to complete SBx + TBx due to some special reasons, and only underwent either SB or TB puncture. The remaining 76 patients underwent SBx + TBx biopsy guiding by MRI-TRUS fusion (Figure 5).

3.2 | Oncological Outcomes

For patients with PI-RADS 4 and 5 lesions, using of TBx + SBx resulted in detection rates of 71.0% and 100% for anyPCa, respectively (Tables 2 and 3). For patients with PI-RADS 3 lesions, the detection rates were 42.1% for anyPCa and 26.3% for csPCa. While, in patients with PI-RADS 4 and

5 lesions, TBx alone achieved a high detection rate (58.1% anyPCa, 51.6% csPCa in PI-RADS 4; 100% anyPCa, 88.5% csPCa in PI-RADS 5). Meanwhile, in PI-RADS 5 patients, TBx alone detected a higher anyPCa rate in comparison to SBx alone (100% vs. 96.2%), achieving an equivalent detection rate of to TBx + SBx (100%) while requiring a lower number of cores (Table 3). As shown in Table 3, we compared the number of positive cases detected by TBx, SBx and TBx + SBx biopsies. In terms of positive cores (Table 4), TBx presented a higher positive rate than SBx in all patients with PI-RADS scores of 3–5. The csPCa detection rate was 69.2% for TBx and 54.5% for SBx in the total number of biopsy cores performed on patients with a PI-RADS score of 5 (Table 4). The result demonstrates the superiority of TBx over SBx in PCa detection.

TABLE 1 | Demographic data.

Parameter	Result
Patients (*n*)	76
Median age, year, M ± SD	70.6 ± 6.3
PI-RADS, *n* (%)	
3	19 (25.0)
4	31 (40.8)
5	26 (34.2)
Median prostate volume, cm^3, M (IQR)	45.6 (33.9, 54.9)
Median tPSA, ng/mL, M (IQR)	15.2 (8.8, 40.3)
Number of MRI targets, *n* (%)	
1	13 (17.1)
2	48 (63.2)
3	15 (19.7)
Preoperative registration time, min, M (IQR)	5.0 (4.4, 6.0)
Operation time, min, M (IQR)	24.8 (23.2, 27.2)

3.3 | Procedural Outcomes

The median preoperative registration time was 5.0 min (IQR: 4.4–6.0) (including automatic reconstruction time+ manually delineating the ROI time 4.5 min (IQR: 3.5–5.1), registration the MRI and TRUS images time 0.8 min (IQR: 0.5–1.0), and the median operation time was 24.8 min (IQR: 23.2–27.2) [including duration of anesthesia 5.2 min (IQR: 4.8–5.8), puncture time 14.8 min (IQR: 13.3–16.0)] (Table 1).

On a pain score by VAS from 0 to 9, majority (65/76) of the patients had VAS 0 to 3, the overall VAS was 2 (0–6), and no one required conversion to general anesthesia (GA) for pain. Of all patients, 15.8% (12/76) developed haematuria, and no episodes of haemochezia or haematospermia were reported. Only one patient experienced urinary retention, 4 patients continued oral antibiotics for 3 days post-surgery, and 2 patients had mild fever (Table 5).

4 | Discussion

In our study, all subjects underwent pre-puncture MRI evaluations to identify suspicious ROIs indicative of PCa. Biopsies were conducted utilizing a novel MRI-TRUS image fusion systems with EM navigation. In conjunction with the standard systematic puncture protocol, 1–3 additional targeted punctures were performed within the ROIs, resulting in a total of 12 + X needle insertions.

In our follow-up, patients did not experience any acute severe complications. Those who experienced pain described it as mild and tolerable. Patients who developed a fever post-surgery saw their symptoms disappear after taking oral antibiotics for 3 days. The complications that did occur were routine and mild in nature.

This study introduced a TP prostate biopsy technique that combined software based MRI-TRUS fusion technology and EM tracking technology. EM tracking technology enables precise planning of the puncture path and accurate localization of target lesions. Software-based MRI-TRUS fusion eliminates the

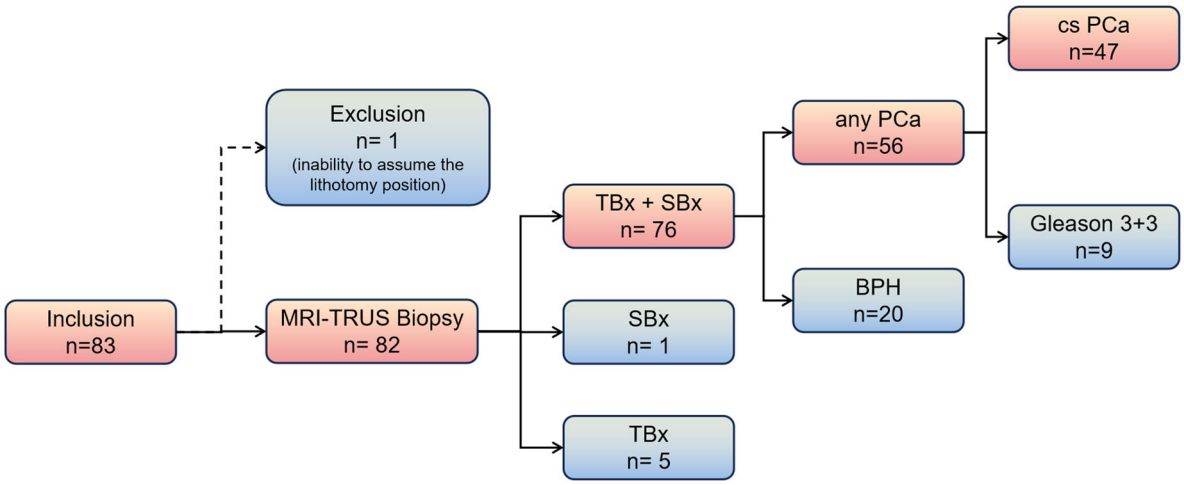

FIGURE 5 | Flowchart of the patient inclusion. [Color figure can be viewed at wileyonlinelibrary.com]

TABLE 2 | Cancer detection rate.

Parameters	AnyPCa rate, *n* (%)	Gleason grade Group 1, *n* (%)	Gleason grade Group 2, *n* (%)	Gleason grade Group 3, *n* (%)	Gleason grade Group 4, *n* (%)	Gleason grade Group 5, *n* (%)
All cases ($n = 76$)	56 (73.7)	9 (16.1)	13 (23.2)	13 (23.2)	9 (16.1)	12 (21.4)
PI-RADS 3 ($n = 19$)	8 (42.1)	3 (37.5)	3 (37.5)	2 (25.0)	0	0
PI-RADS 4 ($n = 31$)	22 (71.0)	3 (13.6)	8 (36.4)	7 (31.8)	2 (9.1)	2 (9.1)
PI-RADS 5 ($n = 26$)	26 (100.0)	3 (11.5)	2 (7.7)	4 (15.4)	7 (26.9)	10 (38.5)

need for cognitive fusion, which may further benefit inexperienced clinicians. In this study, detection rate for any-PCa was 73.7% (56/76) among patients who underwent both TB and SB puncture, and for csPCa was 61.8% (47/76). Paesano et al. [8] conducted a systematic review and meta-analysis of current studies using MRI-TRUS fusion software platforms for TP prostate biopsies (30 articles, 11,313 patients) and the results showed that the cancer detection rate for all PCa was 61.4%, while for csPCa it was 47.8% (Table S4). Some platforms employ robot-assisted techniques for prostate biopsy. Kroenig et al. [21] used the MonaLisa system, which is a software controlled robotic arm, for biopsy in previously biopsy negative men and gained a detection rate of 59.6% and 51.9% for any and significant PCa (Gleason grade ≥ 4), respectively. Rezaee et al. [22] developed a biopsy robot, TRUS-Robot [23], aimed to use a hands-free probe manipulator that moves the probe with the same 4 degrees-of-freedom. TRUS-Robot is designed for TRB based on the mechanical structure, while our proposed method is aimed at TPB, which is gaining preference due to its lower infection risk. The advantage of TRUS-Robot is its hands-free, skill-independent approach. Our system, on the other hand, focuses on automatic surgical planning and navigation. The MRI-TRUS fusion technique combines the detailed representation of MRI with the real-time ultrasound information, and needle-guidance assistive functions to facilitate (manual) puncture. Our system allows flexibility in needle angle and depth selection, especially when targeting lesions in specific, hard-access locations. Comparing with other platforms, such as UroNav [24] and Koelis [25–27], our system utilizes deep neural network for automatic anatomical structure segmentation, i.e., U-Net model for prostate segmentation. In addition, several needle-guidance assistive functions, such as dynamic needle-path and biopsy cores, as well as a safety zone are all visualized to facilitate a fast, accurate, and safe biopsy procedure.

Employing the automatic MRI-TRUS fusion technique for TPB guidance can shorten the surgical time. In this study, the process of image segmentation, lesion delineation, and three-dimensional reconstruction took 4.5 min (IQR: 3.5–5.1). Image registration, on the other hand, only took 0.8 min (IQR: 0.5–1.0). Overall, from data importation to completing the biopsy, it took only 24.8 min (IQR: 23.2–27.2). In the existing reports that using the Koelis platform [28, 29], time for lesion processing for fusion by the urologist cost approximately 4.5–10 min (Table S5). In the study of Immerzeel et al., [11] manually delineating the prostate contour during the biopsy procedure took approximately 10–15 min, which is significantly longer than the 4.5 min (IQR: 3.5–5.1) in our study. The pre-trained CNN-based model can be utilized to automatically segment the prostate contour in MRI and TRUS images, respectively, for later registration. Then, by a rigid registration, the EM tracking coordinate system and the MRI coordinate system are unified for real-time MRI-TRUS fusion, as well as a non-rigid registration method is employed for systematic biopsy core creation. The automatic segmentation and registration procedures reduce the need for manual intervention and thereby achieving time advantage.

Due to inadequate PSA screening within the Chinese population, many patients are diagnosed with metastatic PCa [30]. In our study, patients with a PI-RADS score of 5 had higher PSA

TABLE 3 | Oncological outcomes: per-patient analysis.

Parameters	TBx, *n* (%)		SBx, *n* (%)		TBx + SBx, *n* (%)	
	anyPCa	csPCa	anyPCa	csPCa	anyPCa	csPCa
PI-RADS 3 ($n = 19$)	6 (31.6)	4 (21.4)	7 (36.9)	5 (26.3)	8 (42.1)	5 (26.3)
PI-RADS 4 ($n = 31$)	18 (58.1)	16 (51.6)	21 (67.8)	18 (58.1)	22 (71.0)	19 (61.3)
PI-RADS 5 ($n = 26$)	26 (100)	23 (88.5)	25 (96.2)	23 (88.5)	26 (100)	23 (88.5)

TABLE 4 | Oncological outcomes: per-core analysis.

Parameters	TBx, *n* (%)		SBx, *n* (%)		TBx + SBx, *n* (%)	
	anyPCa	csPCa	anyPCa	csPCa	anyPCa	csPCa
PI-RADS 3	8/38 (21.1)	5/38 (13.2)	24/228 (10.5)	17/228 (7.5)	32/266 (12.0)	22/266 (8.3)
PI-RADS 4	28/64 (43.75)	26/64 (40.6)	82/372 (22.0)	76/372 (20.4)	110/436 (29.6)	102/436 (27.4)
PI-RADS 5	40/52 (76.9)	36/52 (69.2)	179/312 (57.4)	170/312 (54.5)	219/364 (60.2)	206/364 (56.6)

TABLE 5 | Procedural outcomes.

Parameter	Patients
Nausea, *n* (%)	0
VAS, *n* (range)	2 (0–6)
Haematuria, *n* (%)	12 (15.8)
Haemochezia, *n* (%)	0
Haematospermia, *n* (%)	0
Urinary retention, *n* (%)	1 (1.3)
Infection requiring antibiotic treatment, *n* (%)	4 (5.3)
Fever, *n* (%)	2 (2.6)

levels and more advanced clinical staging compared to other populations. As a single-center study with a limited sample size, there is an inherent risk of bias. To mitigate this limitation, and enhance the reliability and generalizability of our findings, we plan to conduct a multi-center analysis in future research.

In this study, the detection rates are relatively high. One reason for these results is that our system uses automatic needle placement and navigation for systematic and target biopsy, ensuring a more uniform needle placement and more precise needle placement compared to cognitive and freehand biopsies. However, on the other, this study is a single-center study with a small sample size, which inevitably introduces some bias and may explain why our PCa detection rates are higher compared to other platform studies. Future research should involve larger, multicenter studies. As the sample size increases, the detection rates for PCa are expected to stabilize, which will help validate the findings and assess the cost-effectiveness of this technology.

5 | Conclusions

In this study, the operation time was reduced and the detection rate of csPCa and PCa was increased, indicated that using automatic MRI-TRUS fusion and navigation technique for TPB was safety and high-efficiency.

Author Contributions

Jie Zhu and Menglin Wu designed this study. Acquisition of data was performed by Jie Zhu, Lu Tang, and Ke Chen. Statistical analysis was performed by Ke Chen, Lu Tang, and Fan Gao. Technical support was offered by Menglin Wu and Sikai Ge. Lu Tang, Shu Zhao, and Baohui Zheng wrote the manuscript with assistance from Jie Zhu, Menglin Wu, and Pablo D. Burstein. Xu Zhang supervised this study. All authors reviewed and edited the manuscript.

Acknowledgments

We would like to express our gratitude to all the patients who participated in this study, their efforts made this study possible. Special thanks are extended to the dedicated healthcare professionals and our research team, they have driven this project forward and their expertize ensured the collection of high-quality data and the provision of exceptional care to the study participants.

Conflicts of Interest

The authors declare no conflicts of interest.

Data Availability Statement

The data that support the findings of this study are available from the corresponding author upon reasonable request.

References

1. R. L. Siegel, K. D. Miller, N. S. Wagle, and A. Jemal, "Cancer Statistics, 2023," *CA: A Cancer Journal for Clinicians* 73 (2023): 17–48.

2. F. Bray, M. Laversanne, H. Sung, et al., "Global Cancer Statistics 2022: GLOBOCAN Estimates of Incidence and Mortality Worldwide for 36 Cancers in 185 Countries," *CA: A Cancer Journal for Clinicians* 74 (2024): 229–263.

3. M. J. Connor, M. A. Gorin, D. Eldred-Evans, et al., "Landmarks in the Evolution of Prostate Biopsy," *Nature Reviews Urology* 20 (2023): 241–258.

4. B. P. Rai, C. Mayerhofer, B. K. Somani, P. Kallidonis, U. Nagele, and T. Tokas, "Magnetic Resonance Imaging/Ultrasound Fusion-Guided

Transperineal Versus Magnetic Resonance Imaging/Ultrasound Fusion-Guided Transrectal Prostate Biopsy-A Systematic Review," *European Urology Oncology* 4 (2021): 904–913.

5. R. Hogenhout, S. Remmers, G. J. L. H. van Leenders, and M. J. Roobol, "The Transition From Transrectal to Transperineal Prostate Biopsy Without Antibiotic Prophylaxis: Cancer Detection Rates and Complication Rates," *Prostate Cancer and Prostatic Diseases* 26 (2023): 581–587.

6. A. R. Meyer, M. Mamawala, J. S. Winoker, et al., "Transperineal Prostate Biopsy Improves the Detection of Clinically Significant Prostate Cancer Among Men on Active Surveillance," *Journal of Urology* 205 (2021): 1069–1074.

7. G. M. Pirola, D. Castellani, L. Orecchia, et al., "Transperineal US-MRI Fusion-Guided Biopsy for the Detection of Clinical Significant Prostate Cancer: A Systematic Review and Meta-Analysis Comparing Cognitive and Software-Assisted Technique," *Cancers* 15 (2023): 3443.

8. N. Paesano, V. Catalá, L. Tcholakian, E. Trilla, and J. Morote, "A Systematic Review of the Current Status of Magnetic Resonance-Ultrasound Images Fusion Software Platforms for Transperineal Prostate Biopsies," *Cancers* 15 (2023): 3329.

9. G. A. Sonn, S. Natarajan, D. J. A. Margolis, et al., "Targeted Biopsy in the Detection of Prostate Cancer Using an Office Based Magnetic Resonance Ultrasound Fusion Device," *Journal of Urology* 189 (2013): 86–92.

10. S. Natarajan, L. S. Marks, D. J. A. Margolis, et al., "Clinical Application of a 3D Ultrasound-Guided Prostate Biopsy System," *Urologic Oncology: Seminars and Original Investigations* 29 (2011): 334–342.

11. J. Immerzeel, B. Israël, J. Bomers, et al., "Multiparametric Magnetic Resonance Imaging for the Detection of Clinically Significant Prostate Cancer: What Urologists Need to Know. Part 4: Transperineal Magnetic Resonance-Ultrasound Fusion Guided Biopsy Using Local Anesthesia," *European Urology* 81 (2022): 110–117.

12. M. Kongnyuy, A. K. George, A. R. Rastinehad, and P. A. Pinto, "Magnetic Resonance Imaging-Ultrasound Fusion-Guided Prostate Biopsy: Review of Technology, Techniques, and Outcomes," *Current Urology Reports* 17 (2016): 32.

13. H. B. Mitchell, *Image Fusion: Theories, Techniques and Applications* (Springer Science & Business Media, 2010).

14. P. Fletcher, M. De Santis, S. Ippoliti, et al., "Vector Prostate Biopsy: A Novel Magnetic Resonance Imaging/Ultrasound Image Fusion Transperineal Biopsy Technique Using Electromagnetic Needle Tracking Under Local Anaesthesia," *European Urology* 83 (2023): 249–256.

15. X. Qin, Z. Zhang, C. Huang, M. Dehghan, O. R. Zaiane, and M. Jagersand, "U2-Net: Going Deeper With Nested U-Structure for Salient Object Detection," *Pattern Recognition* 106 (2020): 107404.

16. Z. Wu and J. M. Sullivan, "Multiple Material Marching Cubes Algorithm," *International Journal for Numerical Methods in Engineering* 58 (2003): 189–207.

17. D. Chetverikov, D. Stepanov, P. Krsek, et al, "Robust Euclidean Alignment of 3D Point Sets: The Trimmed Iterative Closest Point Algorithm," *Image and Vision Computing* 23 (2005): 299–309.

18. J. Kybic and M. Unser, "Fast Parametric Elastic Image Registration," *IEEE Transactions on Image Processing* 12 (2003): 1427–1442.

19. T. H. Kuru, K. Wadhwa, R. T. M. Chang, et al., "Definitions of Terms, Processes and a Minimum Dataset for Transperineal Prostate Biopsies: A Standardization Approach of the Ginsburg Study Group for Enhanced Prostate Diagnostics," *BJU International* 112 (2013): 568–577.

20. G. J. L. H. van Leenders, T. H. van der Kwast, D. J. Grignon, et al., "The 2019 International Society of Urological Pathology (ISUP) Consensus Conference on Grading of Prostatic Carcinoma," *American Journal of Surgical Pathology* 44 (2020): e87–e99.

21. M. Kroenig, K. Schaal, M. Benndorf, et al., "Diagnostic Accuracy of Robot-Guided, Software Based Transperineal MRI/TRUS Fusion Biopsy of the Prostate in a High Risk Population of Previously Biopsy Negative Men," *BioMed Research International* 2016 (2016): 1–6.

22. M. E. Rezaee, K. J. Macura, B. J. Trock, et al., "Likelihood of Sampling Prostate Cancer at Systematic Biopsy as a Function of Gland Volume and Number of Cores," *Prostate Cancer and Prostatic Diseases*. Published ahead of print, January 6, 2024, https://doi.org/10.1038/s41391-023-00780-1.

23. S. Lim, C. Jun, D. Chang, D. Petrisor, M. Han, and D. Stoianovici, "Robotic Transrectal Ultrasound Guided Prostate Biopsy," *IEEE Transactions on Biomedical Engineering* 66 (2019): 2527–2537.

24. S. A. Angileri, L. Di Meglio, M. Petrillo, et al., "Software-Assisted US/MRI Fusion-Targeted Biopsy for Prostate Cancer," *Acta Bio-Medica: Atenei Parmensis* 91 (2020): 2020006.

25. L. Lenfant, C. Beitone, J. Troccaz, et al., "Impact of Relative Volume Difference Between Magnetic Resonance Imaging and Three-Dimensional Transrectal Ultrasound Segmentation on Clinically Significant Prostate Cancer Detection in Fusion Magnetic Resonance Imaging-Targeted Biopsy," *European Urology Oncology* 7 (2024): 430–437.

26. S. Verma, P. L. Choyke, S. C. Eberhardt, et al., "The Current State of MR Imaging-Targeted Biopsy Techniques for Detection of Prostate Cancer," *Radiology* 285 (2017): 343–356.

27. M. Kaneko, D. Sugano, A. H. Lebastchi, et al., "Techniques and Outcomes of MRI-TRUS Fusion Prostate Biopsy," *Current urology reports* 22 (2021): 27.

28. E. Allgood, A. L. Abreu, and S. L. Palmer, "Expedited Workflow for "One-Stop" Magnetic Resonance Imaging and Image Fusion Prostate Biopsy: Implementation and Lessons Learned," *Seminars in Roentgenology* 56 (2021): 406–409.

29. L. Lenfant, C. Beitone, J. Troccaz, et al., "Courbes d'apprentissage de la biopsie ciblée de fusion et de la segmentation échographique de la prostate: une étude monocentrique incluant 14 opérateurs et 1721 Patients," *Progrès en Urologie - FMC* 33 (2023): S108.

30. Y. Zhu, M. Mo, Y. Wei, et al., "Epidemiology and Genomics of Prostate Cancer in Asian Men," *Nature Reviews Urology* 18 (2021): 282–301.

Supporting Information

Additional supporting information can be found online in the Supporting Information section.